International Journal of GEOMATE, Aug., 2022, Vol.23, Issue 96, pp.153-162
ISSN: 2186-2982 (P), 2186-2990 (O), Japan, DOI: https://doi.org/10.21660/2022.96.gxi321
Geotechnique, Construction Materials and Environment

DISCRETE ELEMENT ANALYSIS OF SOIL-PIPE INTERACTION SUBJECTED TO NORMAL AND REVERSE FAULTING

*Yusuke Ono[1]

[1]Faculty of Engineering, Tottori University, Japan

*Corresponding Author, Received: 15 March 2021, Revised: 39 May 2022, Accepted: 12 June 2022

ABSTRACT: Buried pipelines are an essential component of lifelines. However, they are repeatedly damaged by earthquakes. Fault displacement is a significant cause of damage to buried pipelines. In this study, the response of buried pipelines to reverse fault, normal fault, and vertical dislocation was evaluated using the discrete element method (DEM), which can model the details of the nonlinear behavior of the ground. The characteristics of the deformation, bending moment and axial force of the buried pipe for each fault type are clarified about the burial depth. For comparison, a finite element analysis using soil springs was also performed. The results showed that the response of the buried pipe was significantly different from that of the DEM because the deformation of the ground surface could not be considered in the FEM analysis. For finite element analysis with soil springs for the practical design of buried pipes subjected to fault displacement, it is necessary to improve the model of soil springs.

Keywords: Buried pipeline, Soil-pipe interaction, Fault movement, Discrete element method, Finite element method

1. INTRODUCTION

Fault displacement is one of the most common causes of damage to buried pipelines during earthquakes. For example, in the 1971 San Fernando earthquake, more than 1,400 buried water, sewage, and gas pipelines were damaged because of the fault displacement near the ground surface [1]. In the 1999 Chi-Chi earthquake in Taiwan, it was confirmed that some steel pipes subjected to fault displacement were deformed in a z-shape [2]. In the 2014 Kamishiro Fault Earthquake in Nagano Prefecture, a sewer pipe that intersected a reverse fault was damaged by vertical and horizontal displacements of approximately 80 cm and 40 cm, respectively [3]. In the 2016 Kumamoto earthquake, a ductile iron pipe for the water supply crossing the fault in Mashiki Town was bent significantly and detached at the joint [4].

The design of buried pipelines against fault displacement has been developed in the past. Newmark and Hall [5] developed a method to calculate the pipe elongation by considering the non-uniform distribution of frictional forces between the pipe and the surrounding ground under fault displacement. Kennedy et al. [6] extended the method of Newmark and Hall [5] to calculate the bending moment of the pipe. Wang and Yeh [7] proposed a method to model the ground as an elastic spring and a pipe as a beam. Takada et al. [8] developed a finite element analysis method that combines shell and beam elements to accurately evaluate the strains in the pipe at fault crossings. Suzuki [9] developed a method for calculating the deformation and cross-sectional force of a buried pipe subjected to fault displacement by solving the elastic equation of the beam with the range of yielding of the ground as the unknown in a model which treats the buried pipe as an elastic beam and the ground around it as elasto-plastic springs. Talebi and Kiyono [10] developed a new governing equation that includes the exact nonlinear axial and transverse soil-pile interaction terms for a strike-slip fault crossing. At present, finite element analysis, in which the pipe and the ground are modeled as a beam element and nonlinear spring, respectively, is commonly used in design practice to evaluate the cross-sectional force generated in buried pipes subjected to fault displacement. The restoring force characteristics of the nonlinear springs in the ground can be set based on the guidelines released by the American Lifelines Alliance (ALA) [11].

Yoshizaki et al. [12] conducted large-scale experiments to analyze in detail the effects of permanent ground displacement (PGD) on buried steel pipes. Ha et al. [13–15] and Abdoun et al. [16] conducted centrifuge experiments on a reduced model to investigate in detail the relationship between the cross-sectional forces generated in a buried pipe subjected to fault displacement and the characteristics of the pipe and the surrounding soil. In these studies, the effectiveness of the finite element model analysis was verified by comparing it with the experimental results.

Numerical studies have also been conducted to investigate the effects of experimental limitations and many loading conditions. Most of these methods are based on finite element analysis. Finite element analysis was also used in the experimental studies described above [12-16], and the experiment and analysis were consistent. Rahman and Taniyama [17] developed a hybrid model that treated the ground using a discrete element method and the pipe using a

finite element method. They investigated the characteristics of the interaction between them near the fault intersection. They discussed the effects of displacements owing to the reverse and lateral faults and the bending stiffness of the pipe. Because the number of models they analyzed was limited, the discrete element analysis on many models was necessary to clarify the characteristics of the interaction between the pipe and the ground acting on a pipe subjected to fault displacement.

In this study, the deformation and cross-sectional force characteristics of a buried pipeline were analyzed using a three-dimensional discrete element method (DEM). The analyzed models are different from those of Rahman and Taniyama [17]. The fault displacement analyzed was a pure vertical displacement. High-density polyethylene (HDPE) pipes were examined, and their burial depths were 2.4, 4.8, and 7.2 times the outer pipe diameter.

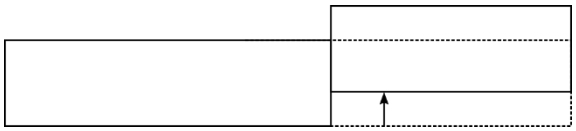

(a) Vertical dislocation

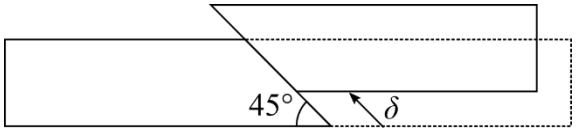

(b) Reverse fault

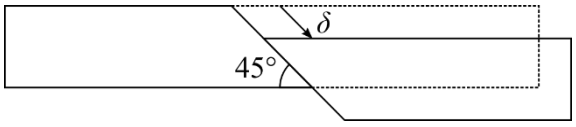

(c) Normal fault

Fig. 1 Types of fault movements considered in the present study.

2. METHOD

2.1 The Discrete Element Method (DEM)

DEM [18] is a popular numerical tool in geotechnical engineering that can directly address the granular properties of the ground. The deformation of the ground is represented by the motion of many rigid bodies. In general, spheres are used as rigid bodies because of their simplicity in detecting contact. In this study, the ground was modeled as a set of spheres.

The contact between spheres is determined by the relationship between their radii and the distance to the center of gravity. When the radii of the two spheres are r_1 and r_2, respectively, and the distance between their centers of gravity is r_{12}, the two spheres are in contact if they satisfy the following relationship:

$$r_1 + r_2 \leq r_{12} \tag{1}$$

When contact occurs, virtual springs and dashpots are generated in the tangential and normal directions of the contact point, respectively, and the contact force acting on the sphere is calculated. The equation of motion of the sphere is as follows:

$$m\ddot{x}_i = F_i \tag{2}$$

where $\boldsymbol{F_i}$ is the *i*-directional component of the sum of all contact forces acting on the sphere; $\boldsymbol{m}$ is the mass of the sphere, and $\ddot{\boldsymbol{x}}_{\boldsymbol{i}}$ is the acceleration. In the DEM, both translational and rotational motions of the object are considered. The equation of motion for rotation is given by:

$$\boldsymbol{I_i\ddot{\omega}_i = M_i} \tag{3}$$

Where the index *i* represents the central axis of rotation, $\boldsymbol{I_i}$ is the rotational inertia, $\ddot{\boldsymbol{\omega}}_{\boldsymbol{i}}$ is the rotational acceleration, and $\boldsymbol{M_i}$ is the moment.

The maximum shear force F^s_{max} is determined as follows:

$$F^s_{max} = \mu F^n \tag{4}$$

where F^n and μ are the normal contact force and frictional coefficient between the spheres, respectively.

The open-source software Yade 2020.01a [19] was used in this study. Spherical elements were used for the ground, while a chained cylinder element was used to represent the buried pipe. The chained cylinder model deforms according to the elastic beam theory. However, since the chained cylinder model [20], [21] implemented in the Yade does not support a hollow cross-section such as a pipe, the source code required slight modification.

2.2 Analytical Model

The ground model, whose length, width, and height were 14 m, 1 m, and 1 m, respectively, was placed in a rigid box, as shown in Fig. 2. The box was divided into two parts, one of which was fixed, while the other was movable. For normal or reverse fault analysis, the fault plane was tilted by 45° to the fixed side. The movement of the fault was simulated by moving the movable side of the box at a constant speed of 0.5 m/s. The maximum fault movement δ is 0.30 m. The box was modeled using the facet elements provided by Yade. In the actual analytical mode, a flat plate was placed at the bottom of the box to prevent the spherical elements from spilling

through the gap created by the movement of the fault.

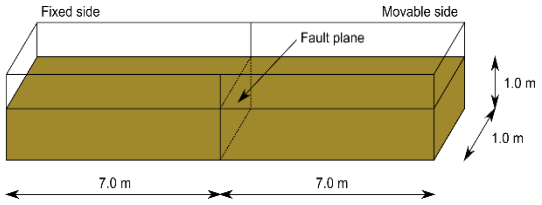

(a) Vertical dislocation type

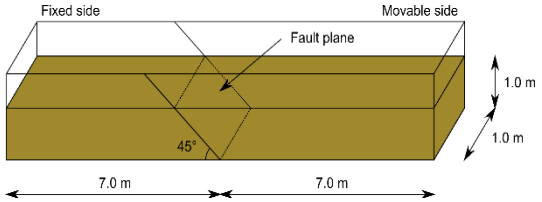

(b) Normal and reverse fault types

Fig. 2 Dimension of the analytical model.

Table 1 summarizes the parameters of the spherical elements. The spherical elements used in the analysis were all equal in size. When analyzing the ground using the DEM, it is desirable to keep the size of the spherical elements as small as possible. However, if the size of the spherical elements is too small, the number of required elements becomes too large, and the analysis cannot be performed realistically. Therefore, in this study, the spherical element was assigned a diameter of 0.04 m, as a guideline to ensure the complete analysis of one case in a few hours. Hence, 319,726 spherical elements were used.

An HDPE pipe with an outer diameter of 0.125 m (whose parameters are listed in Table 2) is analyzed. Although HDPE is a strain-rate-dependent material, it is treated as an elastic material. The variation in the cross-sectional shape of the pipe was neglected. The modeled pipe was buried horizontally in the center of the width, at the specified depth, and its ends were rigidly attached to the walls of the rigid box.

The frictional coefficient μ between the surface of the pipe and spherical elements was determined by Eq. (5) using the internal friction angle betweenbetweenφ between the spherical elements,

$$\mu = \tan f\varphi \tag{5}$$

where f, the coating coefficient of the pipe, was assigned a value of 0.6 according to the ALA guidelines [11].

2.3 Simulation Cases

Nine cases, as listed in Table 3, were analyzed. The three types of faults were vertical longitudinal dislocation, 45-degree reverse fault, and 45-degree normal fault, as shown in Fig. 1. The pipe burial depths (distance from the ground surface to the central axis of the pipe) were 0.30 m, 0.60 m, and 0.90 m.

Table 1 Parameters for the spherical elements

Parameter	Value
Diameter (m)	0.040
Density (kg/m^3)	2.4×10^3
Elastic modulus (N/m^2)	3.0×10^7
Poisson's ratio	0.15
Internal friction angle	35.0°

Table 2 Parameters for the pipe model

Parameters	Value
Diameter (m)	0.125
Thickness (m)	0.0114
Elastic modulus (N/m^2)	1.0×10^9
Poisson's ratio	0.46

Table 3 Summary of the analytical cases

Case	Fault type	Burial depth (m)
111	Vertical dislocation	0.30
112	Reverse fault	0.30
113	Normal fault	0.30
121	Vertical dislocation	0.60
122	Reverse fault	0.60
123	Normal fault	0.60
131	Vertical dislocation	0.90
132	Reverse fault	0.90
133	Normal fault	0.90

The burial depth is defined as the depth from the ground surface to the centerline of the pipe.

2.4 Simulation Procedure

First, spherical elements of a specified size were randomly generated in the prepared box, deposited under gravity, and stabilized until their motion settled sufficiently. The number of spherical elements to be generated was adjusted by trial and error to ensure that the height of the ground after stabilization was approximately 1.0 m. At this point, the friction between the elements was set to zero so that the spherical elements would be as dense as possible. Next, the spherical elements were removed from the buried position of the pipe, and the pipe was placed in the vacant space. After confirming that the motion of the spherical elements was sufficiently settled under the action of gravity, the fault displacement was applied. Figure 3 shows the ground model just before the fault displacement was applied. The spherical elements are colored in a grid pattern to identify the deformation of the ground. The porosity of the ground was 0.490.

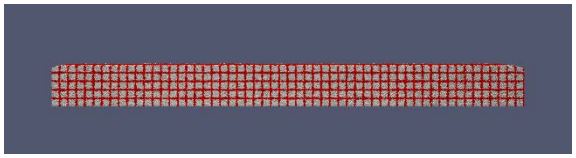

Fig. 3 Side view of the ground model before applying the fault movement

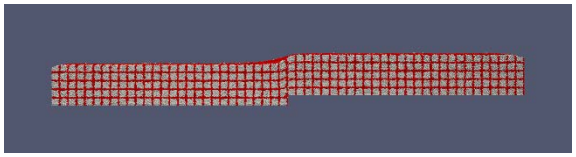

(a) Vertical dislocation

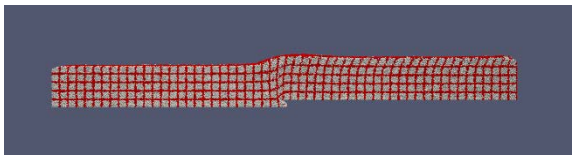

(b) Reverse fault

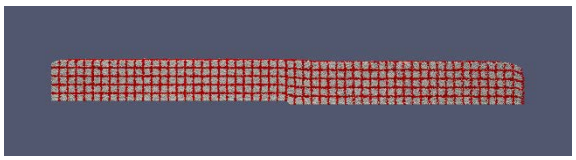

(c) Normal fault

Fig. 4 Deformation of the ground models after applying the fault movement

3. RESULTS AND DISCUSSION

3.1 Deformation of the Ground Model

Figure 4 shows a side view of the ground model after a fault displacement of 0.30 m was applied. There are some differences in the ground surface deformation depending on the burial depth of the pipe. However, a pipe with a burial depth of 0.30 m is shown here as an example. In the model with vertical dislocation, a gentle slope was formed just above the fault because of the flow of spherical elements. In the model with reverse faulting, the ground is significantly compressed above the fault plane. The ground on the fixed side was hardly deformed, while the ground on the moving side was deformed over a wide area. In particular, the ground near the surface was deformed to the rightmost boundary. In the case of a normal fault, the subsidence of the ground surface was smaller than that in the vertical direction at the bottom of the moving side, because the ground could not sufficiently follow the movement of the fault and its pores enlarged. Near the right boundary, the ground could not keep up with the movement of the boundary, resulting in a gap between the wall and the ground.

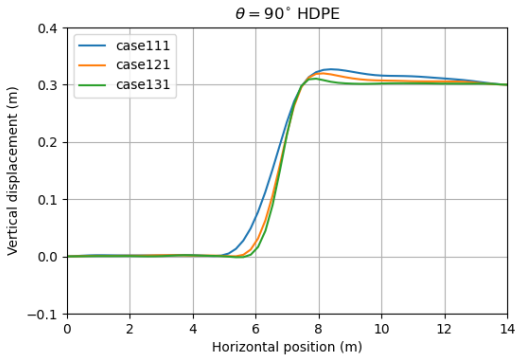

(a) Vertical dislocation

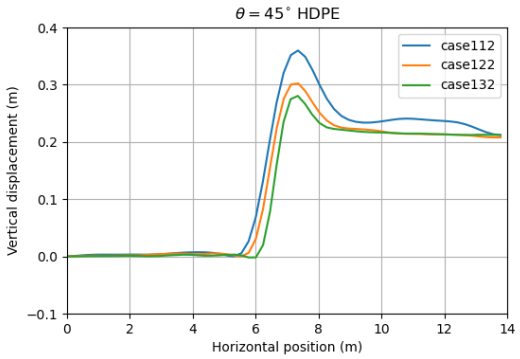

(b) Reverse fault

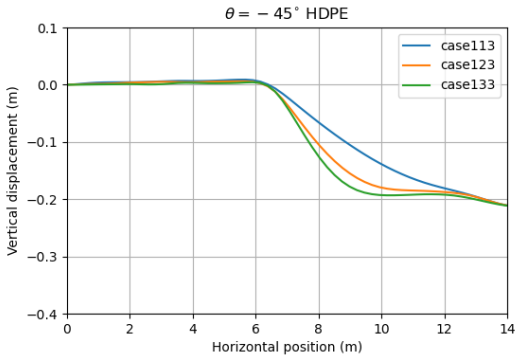

(c) Normal fault

Fig. 5 Deformation of the pipe along the axial direction.

3.2 Deformation of the Pipe

The deformation of the buried pipe when the displacement of each fault movement pattes3rn reaches 0.30 m is shown in Fig. 5. The pipe exhibits a characteristic deformation according to the fault pattern.

In the case of vertical dislocation, the pipe deformed slightly upward from just above the fault to the moving side. The deformation of the pipe on the fixed side occurred only near the fault. The vertical upward displacement of the pipe is more significant at shallower burial depths because the downward force acting on the pipe was smaller. In the case of reverse faulting, the pipe bends upwards significantly

on the moving side near the fault.

In the case of reverse faulting, the pipe bends upward significantly on the moving side of the ground near the fault. In this case, the pipe is compressed by the fault movement, and thus its upward deformation is larger. Since the downward restraining force acting on the pipe is smaller at shallower burial depths, the pipe is bent to a larger extent. In the case of the shallowest burial depth, the pipe deforms even near the boundary of the moving box (left side of the figure), indicating that the boundary affects the analysis results.

In the model with normal faults, the pipe deforms gently, unlike in the models with the other two fault types. For the shallowest burial depth case, the deformation of the pipe continues to the left boundary, unlike the cases with different burial depths.

3.3 Bending Moment of the Pipe

The bending moment generated in the pipe is illustrated in Fig. 6. When the vertical discrepancy is given, the bending moment on the fixed side is positive while that on the moved side is negative. The bending moment of the pipe is almost zero at the intersection with the fault and larger at greater burial depths. The point where the bending moment is the largest on the fixed side is farther from the fault location as the burial depth becomes shallower. On the other hand, the position of the maximum bending moment on the moving side remains almost the same regardless of the burial depth. The maximum value of the bending moment was larger on the moving side than on the fixed side.

The shape of the distribution of the bending moment of the pipe in the results of reverse faulting resembles that of the results of vertical dislocation. The position where the bending moment becomes zero is almost the same. The bending moment of the pipe is positive on the fixed side and negative on the moving side. Its maximum magnitude was larger when the pipe was buried deeper at both the fixed and moving sides. The position where the maximum bending moment appears is constant regardless of the burial depth on the fixed side, while it approaches the fault on the moving side as the burial depth increases.

In the case of normal faulting, the bending moment generated in the pipe is smaller than that obtained with vertical dislocation or reverse faulting. It is negative for the fixed side and positive for the moving side, which is opposite to the other two cases. The tendency of the magnitude of the bending moment to increase with the depth of burial is the same as in the other cases.

3.4 Axial Force of the Pipe

Figure 7 shows the axial force of the pipe. The axial force was positive in tension and negative in compression. In the models with a vertical dislocation and normal fault, tensile forces act on the pipe. On the other hand, compressive forces act on the pipe in the model with reverse faults.

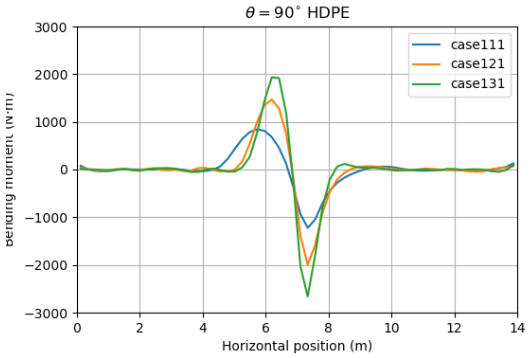

(a) Vertical dislocation

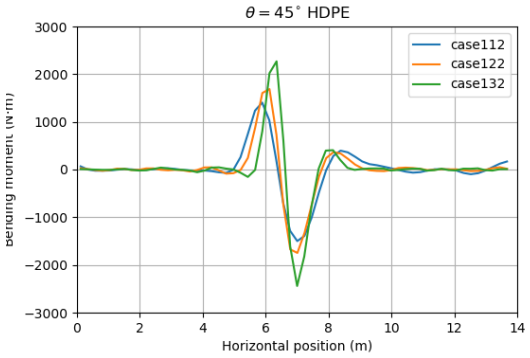

(b) Reverse fault

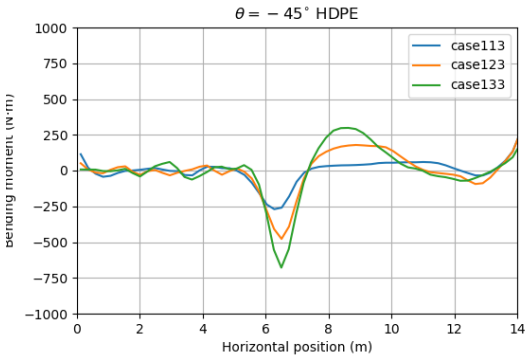

(c) Normal fault

Fig. 6 Bending moment of the pipe at the different burial depths.

In the model with vertical dislocation, the tensile force acting on the pipe was large near the fault and decreased as it approached the lateral boundary. The axial force is almost constant near the fault, indicating that the reaction force acting on the pipe has reached its maximum value. Near the fault, the axial force increased with the depth of the pipe. The difference in the slope of the axial force graph shows that the reaction force acting on the pipe increases with the pipe burial depth. The axial force decreased with

burial depth near the right and left boundaries. The axial force at the right boundary exceeds that at the left boundary, possibly because of dynamic effects.

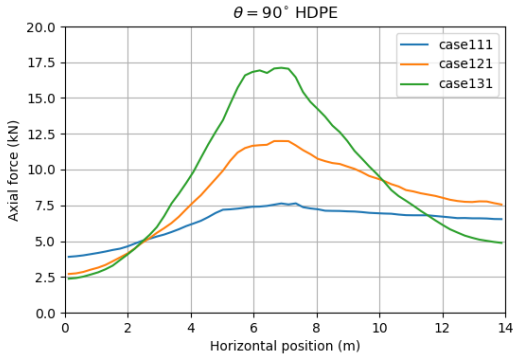

(a) Vertical dislocation

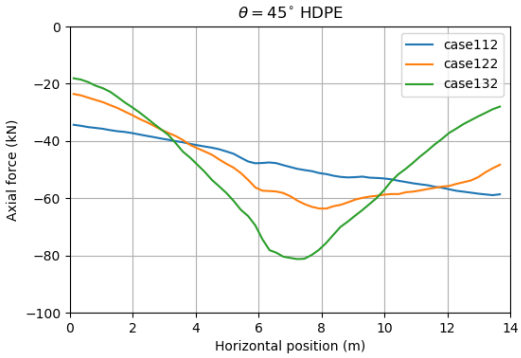

(b) Reverse fault

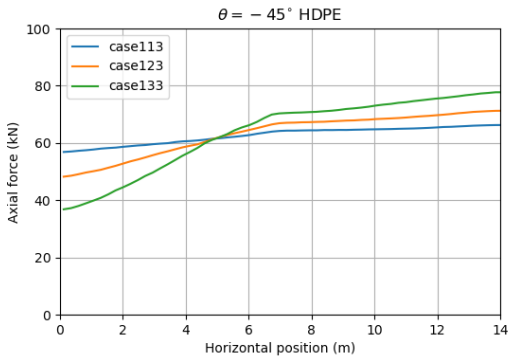

(c) Normal fault

Fig. 7 Axial force of the pipe at the different burial depths.

In the reverse fault model, the compressive force on the pipe at the intersection with the fault was the largest in the deepest case132. In case 132, where the depth of burial is the maximum, the compressive force on the pipe is the largest at the intersection with the fault, and the graph flattens near the maximum compressive force, indicating that the ground reaction force has reached its maximum. On the other hand, in case112, where the soil cover is the shallowest, the compressive force increases monotonically from the left boundary to the right boundary, displaying a trend different from the case with the deepest burial depth. In the intermediate case122, the compressive force is the highest near the fault and decreases toward the boundary. The rate of change of the compressive force differs between the fixed and moving sides.

In the normal fault model, the tensile force is the highest at the boundary on the moving side and decreases towards the boundary on the fixed side. The rate of change of tensile force differs on both sides of the intersection of the pipe and fault, and the rate of change of the tensile force on the moving side is lower than that on the fixed side.

3.5 Comparison with the Finite Element Analysis

The deformations, bending moments, and axial forces of the pipes obtained using DEM were compared with the results obtained by finite element analysis. The software OpenSeesPy [22], which enables the control of OpenSees [23] using Python script, was used for finite element analysis.

3.5.1 Finite element model

The pipe was modeled as an elastic beam element and the ground as soil springs. The ground springs were applied in the axial and transverse directions. The transverse soil springs generate reaction forces against the upward or downward movement of the pipe. Both ground springs were modeled as elastic-perfectly plastic models following the ALA guidelines [11]. The maximum force F_{max} and yield displacement δ_y of each soil spring were determined as follows, according to the ALA guidelines [11].

The maximum force per unit length F_{max} and the yield displacement δ_y (m) in the axial direction are given by

$$F_{max} = \pi D H \bar{\gamma} \frac{1+K_0}{2} \tan(f\phi) \quad (6)$$

$$\delta_y = 0.003 \quad (7)$$

where D, H, $\bar{\gamma}$, K_0, ϕ, and f are the outer diameter of the pipe, depth of the centerline of the pipe from the ground surface, unit weight of the ground, coefficient of pressure at rest, internal friction angle of the ground, a factor of pipe coating (assigned a value of 0.6), respectively.

For the vertical uplift soil spring, the maximum force per unit length and yield displacement δ_y is given by

$$F_{max} = \left(\frac{\phi H}{44D}\right) \bar{\gamma} H D \quad (8)$$

$$\delta_y = 0.01H \quad (9)$$

The maximum force per unit length F_{max} and the yielding displacement δ_y for the vertical bearing soil

spring are,

$$F_{\max} = e^{(\pi \tan\phi)} \tan^2\left(45 + \frac{\phi}{2}\right) + e^{(0.18\phi - 2.5)} \gamma \frac{D^2}{2} \quad (10)$$

$$\delta_y = 0.1D \quad (11)$$

This finite element analysis model neglects the coupling of the bending moment and axial force in the pipe. In addition, the coupling between the axial (horizontal) and transverse (vertical) ground springs is not considered.

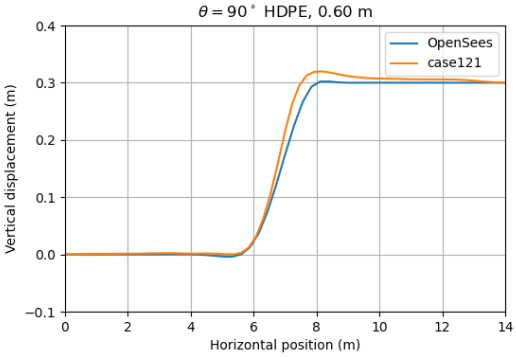

(a) Vertical dislocation

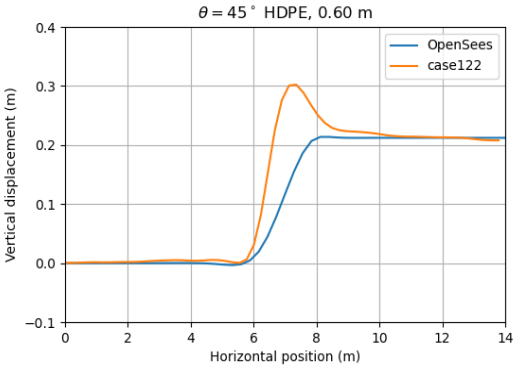

(b) Reverse fault

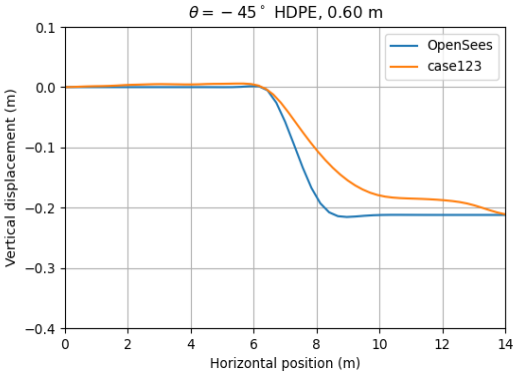

(c) Normal fault

Fig. 8 Comparison of the pipe deformation obtained using DEM to that obtained using FEM

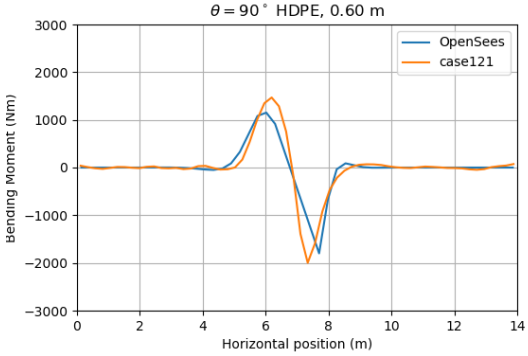

(a) Vertical dislocation

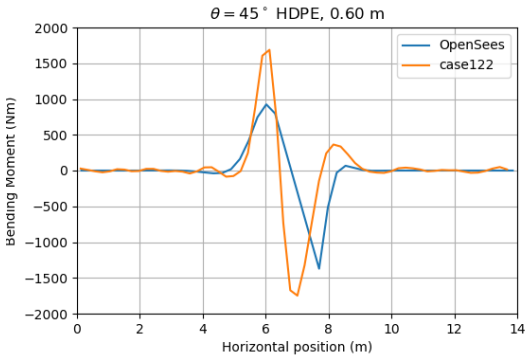

(b) Reverse fault

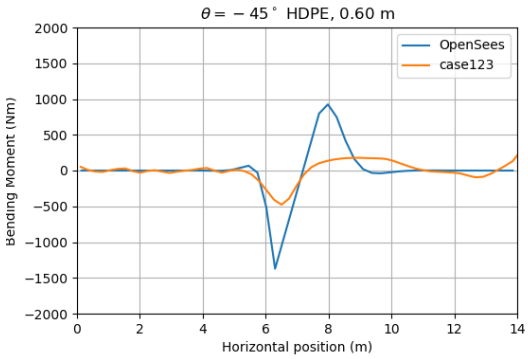

(c) Normal fault

Fig. 9 Comparison of the bending moment of the pipe obtained using DEM to that obtained using FEM

3.5.2 Results

Figure 8 shows the pipe deformation for each fault type. For the vertical dislocation model, the results of the DEM and the finite element method (FEM) are in general agreement. However, in the discrete element analysis, the pipe was slightly raised at the fault intersection. The results of the DEM and FEM for pipe deformation in the model with reverse faulting differ significantly. The upward convex deformation of the pipe at the fault intersection observed in the DEM results was not observed in the FEM results because the finite element method does not consider account the effect of the axial force on the bending of the pipe. For normal faults, the deformations of the

pipes on the moving side differ from each other. The FEM results show that the pipe is pushed down to a deeper position compared to the DEM results. This indicated that in FEM, the ground above the moving pipe exerts excessive force on the pipe.

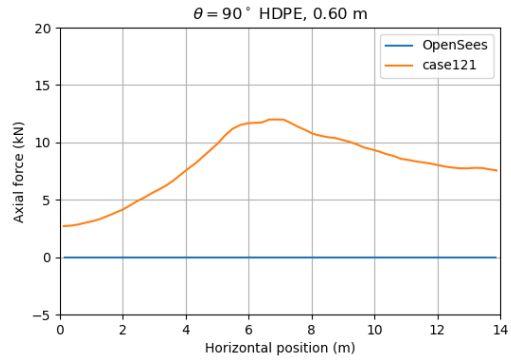

(a) Vertical dislocation

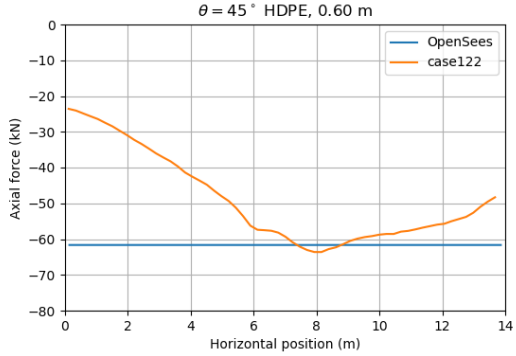

(b) Reverse fault

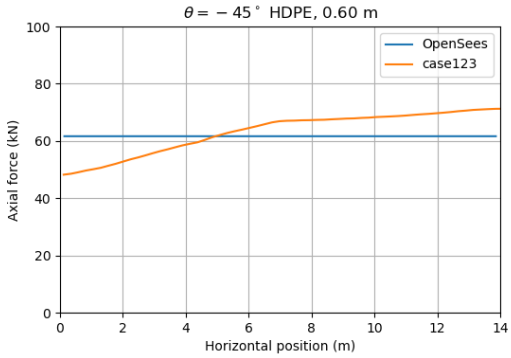

(c) Normal fault

Fig. 10 Comparison of axial force of the pipe obtained using DEM to that obtained using FEM

Figure 9 compares the distribution of the bending moments of the pipes. The DEM and FEM results are very similar for the bending moment of the vertical dislocation model. For the reverse fault model, the peak values of the bending moments were different for both the fixed and moving sides. In particular, the peak bending moment on the fixed side was much lower in the FEM than in the FEM. For the peak bending moment caused by the normal fault, the FEM results are higher than the DEM results, contrary to the case of the reverse fault.

Figure 10 shows the axial force generated in the pipe. In this figure, the axial force obtained from the results of the DEM varies along the pipe, while that obtained using FEM remains constant. This is because the axial slip between the pipe and ground occurs at a relative displacement as small as 3 mm in the ground spring used in the finite element analysis, and the effect of the force acting perpendicular to the axis of the pipe on the maximum friction force is neglected.

4. CONCLUSIONS

In this study, the deformation, bending moment, and axial force of the buried pipe were determined for vertical dislocation, reverse fault, and normal fault using DEM. The results of the calculations are summarized as follows:

1. For reverse faults, the buried pipe bends toward the ground surface near the fault intersection in the hanging wall. The deformation of the buried pipe increases with a decrease in the burial depth.
2. Regardless of the fault type, the bending moment generated in the buried pipe is not symmetrical concerning the fault plane. The maximum value of the bending moment increases with the burial depth.
3. In both the normal fault and vertical dislocation cases, tensile axial forces act on the buried pipe, but the shape of their distribution is different.

A finite element method (FEM) analysis was also performed, in which the ground was modeled as a spring and the buried pipe as a beam. The results obtained by FEM were compared with those obtained by DEM. The results obtained can be summarized as follows:

1. For the vertical dislocation cases, the deformation and bending moment of the buried pipe showed good agreement between the DEM and FEM results, respectively.
2. For normal faults, the deformation of the buried pipe obtained by FEM analysis is larger than that by DEM analysis.
3. For reverse faults, the FEM analysis cannot reproduce the deformation of the buried pipe that extends toward the ground surface. This is because FEM using ground springs does not take into account the effect of deformation of the ground surface.
4. For reverse faults, the deformation of the buried pipe obtained by FEM analysis is smaller than that obtained by DEM analysis.
5. For reverse faults, the FEM analysis cannot reproduce the deformation of the buried pipe that extends toward the ground surface. This is because FEM using ground springs cannot take into

account the effect of deformation of the ground surface.

In general, the results of ground deformation analysis using DEM depend on the size of the elements used. Therefore, it is necessary to confirm that the findings of this study do not largely depend on the size of the spherical elements. In addition, further investigation of the axial force is needed because the FEM analysis conducted in this study did not use the ground spring in the pipe axial direction.

5. ACKNOWLEDGMENTS

This work was supported by MEXT KAKENHI Grant Number JP20H00258.

6. REFERENCES

[1] McCaffrey M. A., and O'Rourke T. D., Buried pipeline response to reverse faulting during the 1971 San Fernando Earthquake., ASME, PVP. Vol.77, 1983, pp.151-159.

[2] Shih B.J., and Chang C.H., Damage survey of water supply systems and fragility curve of PVC water pipelines in the Chi–Chi Taiwan earthquake, Natural Hazards, Vol. 37, No. 1-2, 2006, pp. 71-85.

[3] Japan Association for Earthquake Engineering, Report of the investigation team on the 2014 earthquake in northern Nagano Prefecture, 2015 (in Japanese).

[4] Committee for the Evaluation of Seismic Performance of Polyethylene Pipes for Water Distribution, Guide to seismic design of polyethylene pipes for water distribution, Reference Materials, 2018, pp. 46-47 (in Japanese).

[5] Newmark N.M., and Hall W.J., Pipeline design to resist large fault displacement, Proc. of US national conference on earthquake engineering, 1975, pp. 416-425.

[6] Kennedy R.P, and Kincaid R.H., Fault crossing design for buried pipelines for seismic-induced ground distortions, Proceedings of 4th National Congress on Pressure Vessel and Piping Technology, 1983, pp. 1-24.

[7] Wang L.R.L., and Yeh Y.H., A refined seismic analysis, and design of buried pipeline for fault movement, Earthquake Engineering & Structural Dynamics, Vol. 13, No. 1, 1985, pp. 75-96.

[8] Takada S., Hassani N., and Fukuda K., A new proposal for simplified design of buried steel pipes crossing active faults, Earthquake engineering & structural dynamics, Vol. 30, No. 8, 2001, pp. 1243-1257.

[9] Suzuki T., Approximate calculation method for beam model supported by inelastic springs in enforced displacement, Doboku Gakkai Ronbunshu, Vol. 2001, No.689, 2001, pp. 109-116 (in Japanese).

[10] Talebi F. and Kiyono J., A refined nonlinear analytical method for buried pipelines crossing strike-slip faults, Earthquake Engineering and Structural Dynamics, Vol. 50, No. 11, 2021, pp. 2915-2938.

[11] American Lifelines Alliance, Seismic guidelines for water pipelines, 2005.

[12] Yoshizaki K., O'Rourke T.D., and Hamada M., Large scale experiments of buried steel pipelines with elbows subjected to permanent ground deformation, Structural Engineering/Earthquake Engineering, Vol. 20, No. 1, 2003, pp. 1-11.

[13] Ha D. et al., Buried high-density polyethylene pipelines subjected to normal and strike-slip faulting—A centrifuge investigation, Canadian Geotechnical Journal, Vol. 45, No. 12, 2008, pp. 1733-1742.

[14] Ha D. et al., Centrifuge modeling of earthquake effects on buried high-density polyethylene (HDPE) pipelines crossing fault zones, Journal of Geotechnical and Geoenvironmental Engineering, Vol. 134, No. 10, 2008, pp. 1501-1515.

[15] Ha, D. et al., Earthquake faulting effects on buried pipelines–case history and centrifuge study, Journal of Earthquake Engineering, Vol. 14, No. 5, 2010, pp .646-669.

[16] Abdoun, T.H., et al., Factors influencing the behavior of buried pipelines subjected to earthquake faulting, Soil Dynamics and Earthquake Engineering, Vol. 29, No. 3, 2009, pp. 415-427.

[17] Rahman M.A., and Taniyama H., Analysis of a buried pipeline subjected to fault displacement: A DEM and FEM study, Soil Dynamics and Earthquake Engineering, Vol. 71, 2015, pp. 49-62.

[18] Cundall P.A., and Strack O.D.L., A discrete numerical model for granular assemblies, Géotechnique, Vol. 29, No. 1, 1979, pp. 47-65.

[19] Kozicki J. , and Donze F.V., YADE-OPEN DEM: An open-source software using a discrete element method to simulate granular material, Engineering Computations, Vol. 27, No. 7, 2009, pp. 786-805.

[20] Effeindzourou A., et al., A general method for modeling deformable structures in DEM, Proc. of the IV International Conference on Particle-Based Methods: fundamentals and applications, 2015.

[21] Wu W., et al., the effect of vegetation on the stability of soil slopes: numerical aspect, Recent

advances in modeling landslides and debris flows, 2015, pp. 163-177.
[22] Zhu M., McKenna F., and Scott M.H., OpenSeesPy: Python library for the OpenSees finite element framework, SoftwareX, Vol. 7, 2018, pp. 6-11.
[23] McKenna F., Scott M.H., and Fenves G.L., Nonlinear finite-element analysis software architecture using object composition, Journal of Computing in Civil Engineering, Vol. 24, No. 1, 2010, pp. 95-107.